AN ABSTRACT OF THE THESIS OF

Kevin Tyler Carpenter for the degree of Master of Science in Mechanical Engineering presented on March 22, 2019.

Title: The Applicability of Linear Elastic Fracture Mechanics to Compressive Damage of the Carbon Fiber Reinforced Plastic Matrix.

Abstract approved:

_____

John P. Parmigiani

With the widespread replacement of aluminum with composite materials, particularly in aircraft structures, the lack of comprehensive understanding of these materials is unsettling. The complex nature of these materials, with respect to isotropic aluminum, makes the prediction of their mechanical response equally complex. The failure of carbon fiber reinforced plastic composites has been categorized into fiber tension, fiber compression, matrix tension, and matrix compression. The first three of these failure modes have been explored rigorously, and the behavior is fairly well established. Matrix compression, however, has not been investigated as thoroughly and assumptions have been made throughout research and industry that had not been validated. This research served to identify, through experimental techniques, a test specimen suitable for isolating the matrix compression damage response. After the development of a suitable specimen, the investigation to the validity of the assumptions commonly made regarding matrix compression loading was conducted. It was often assumed that the matrix under compressive loads followed the

relationships established by linear elastic fracture mechanics, which has never been experimentally demonstrated; the work presented here does so. Through specimens of variable notch lengths, the failure load was related to the corresponding notch length, and the relationship observed was compared to the relationship defined by linear elastic fracture mechanics. The defined relationship would have a linear slope of -0.5, and the data reported here showed a linear trend with a slope of -0.54 with error bars that included the linear relationship having a slope of -0.5, thus confirming the applicability of linear elastic fracture mechanics to the matrix in compression. A method was also proposed to calculate the critical strain energy release rate for matrix compression—a value that is often considered negligible or approximated from other parameters for implementation into damage models. Using a displacement-controlled definition of the critical strain energy release rate, a value of 65.51-lb/in with a standard deviation of about 18.66-lb/in, comparing well with a reported value. A final observation that further supported the need for matrix compression investigations was the post-damage initiation behavior in the matrix; after damage initiated, the fractured surfaces continued to support load—in continuum damage mechanics models currently implemented, the load-carrying ability is linearly degraded to zero. Matrix compression must be researched further.

The Applicability of Linear Elastic Fracture Mechanics to Compressive Damage of the Carbon Fiber Reinforced Plastic Matrix

by
Kevin Tyler Carpenter

A THESIS

submitted to

Oregon State University

in partial fulfillment of
the requirements for the
degree of

Master of Science

Presented March 22, 2019
Commencement June 2019

Master of Science thesis of Kevin Tyler Carpenter presented on March 22, 2019

APPROVED:

Major Professor, representing Mechanical Engineering

Head of the School of Mechanical, Industrial, and Manufacturing Engineering

Dean of the Graduate School

I understand that my thesis will become part of the permanent collection of Oregon State University libraries. My signature below authorizes release of my thesis to any reader upon request.

Kevin Tyler Carpenter, Author

ACKNOWLEDGEMENTS

I would like to express the most sincere appreciation to Dr. John Parmigiani for taking the time to guide me through the transition of waiting for the answer in a classroom to finding the answer on my own in a laboratory. His leadership pushed me to be a better student, researcher, and engineer. I would also like to thank the members of the lab (past and present): Nicholas Aerne, Taylor Rawlings, David Plechaty, Patrick Sellars, and Kevan Gahan, who were there to brainstorm ideas whenever problems arose. Finally, I would like to thank Ashley for always being there to encourage me, and for pushing me to strive for excellence.

CONTRIBUTION OF AUTHORS

Dr. John Parmigiani was involved in providing feedback and support throughout Chapters 1-5. Tim McKinley provided significant contributions to Chapter 3. David Plechaty was involved in, and provided assistance to Chapters 3, 4, and 5.

TABLE OF CONTENTS

TABLE OF CONTENTS (Continued)

Page

LIST OF FIGURES

Figure Page

LIST OF TABLES

DEDICATION

The following document is dedicated to Mr. Bill. We did it; I hope I grew up to be a man you would be proud of.

The Applicability of Linear Elastic Fracture Mechanics to Compressive Damage of the Carbon Fiber Reinforced Plastic Matrix

Chapter 1

1 Introduction

The use of composite materials has been expanding across industries—from sports equipment to aircraft vehicles, which has demanded confidence in designs. Traditionally, many aircraft structures have been designed with aluminum. The mechanics of aluminum have been explored thoroughly, and is a well understood material. As the field of materials science engineering grows and new materials are developed, unique mechanical characteristics can attract considerable attention. Carbon fiber reinforced plastic (CFRP) composites are types of materials that have attracted such attention, particularly in the aerospace industry, due to their high strength-to-weight ratios [1, 2]. CFRP composites consist of carbon fibers secured in a plastic matrix for reinforcement. While CFRP's have been around for several decades [3], the inhomogeneity and anisotropy of laminates make the mechanical behavior complex, thus, the modes of their mechanical failure are still under investigation [4]. Because aircraft structures must adhere to specific safety requirements and regulations, the material behavior used must be well understood.

As a cost-effective design tool, instead of expensive experimental investigations of the mechanical response of a composite structure, industry professionals will evaluate their designs in a finite element modeling software, like Abaqus or ANSYS, to simulate an environment. Finite Element Analysis (FEA) is a useful tool to model complex geometries and unique loading conditions to predict the mechanical response. Aerospace structures and components are large and expensive, making computer models and simulations a desirable alternative to large-scale mechanical testing. Of course, FEA is not a sufficient substitute for large-scale certification testing, but it helps eliminate the iterative, trial-and-error design approach. Because the physics of the failure of CFRP composites are still under investigation, the question of the reliability of FEA models for composites has been raised.

Composites can experience several different damage mechanisms, both isolated and combined, including fiber-matrix pullout, fiber breaking, fiber kinking/buckling, matrix cracking or yielding, and delamination. There are many tools that one can utilize in FEA software to model damage; one model that has been used extensively is the continuum damage mechanics model [5, 6]. This model is desirable because of how the damage is applied to the part: the damage is smeared over the damage region, eliminating the need to model specific modes of failure (e.g. interactions between particles within the material). Hashin [7] categorized damage of composites into four main failure modes: fiber tension, fiber compression, matrix tension, and matrix compression, and established damage initiation criteria for each of the modes based on material properties, which are widely used in industry. Layczyk and Hurtado [2]

used Hashin's damage initiation criteria to develop a damage model for CFRP's in the context of continuum damage mechanics, which required inputs of material properties for each of the four failure modes, and progressed damage based on a linear stiffness degradation technique.

Of the four failure modes identified by Hashin, the first three have been studied rigorously, while very little research has been devoted to matrix compression. This lack of understanding can lead to over-conservative designs, or very dangerous designs—in the aerospace industry, conservative designs mean more expensive and heavier aircraft, and dangerous designs can be lethal. The Federal Aviation Administration (FAA) and aerospace industry partners have created two research institutions: the Center of Excellence for Advanced Materials in Transport Aircraft Structures (AMTAS), and the Center of Excellence for Composites and Advanced Materials (CECAM) to develop a more concrete understanding of composite materials for safety and certification. This research serves as a part of the center of excellence for AMTAS.

Chapter 2

2 Literature Review

2.1 Fiber Tension and Fiber Compression

In general, a CFRP fiber tension study consists of a laminate with all 0° fibers; that is, all of the fibers in a test specimen are aligned in one direction, with a tensile (or compressive) load applied along that direction. Pinho et al [8] explored methods to directly measure fracture toughness values associated with fiber tensile failure, as well as compressive fiber kinking for carbon fiber composites. Through compact tension (CT) and compact compression (CC) specimens, strain fields were obtained using digital image correlation (DIC), and critical strain energy release rates were determined for initiation, and, in the case of tension, for propagation. In another study by Soutis et al [9], unidirectional specimens were loaded in compression (fiber compression), and investigated for the dominating failure mechanism; it was determined that fiber microbuckling occurs and initiates the damage process. Soutis used Linear Elastic Fracture Mechanics (LEFM) relationships to predict the damage response of fiber compression and were accurate to experimental results within 10%. Soutis's study was extended into work by Sutcliffe et al [10], who were able to describe the mechanisms of the propagation of fiber compression damage. Phillips [11] also showed that LEFM laws could be applied to laminates with cracks

perpendicular to fiber direction (fiber tension). Other fiber compression damage investigations can be seen in literature [12-21].

2.2 Matrix Tension

The isolation and investigation of the matrix under a tensile load has also been studied thoroughly (90° fiber orientation: a tensile load applied perpendicular to the fiber direction). It was concluded by Wu [22] that the laws of LEFM, as they are applied to isotropic materials, are applicable to fiber-reinforced plastics when the crack is oriented parallel to the fiber direction, and a tensile load is applied in the transverse (matrix tension) direction. Waddoups et al [23] stated that the applicability of fracture mechanics to unidirectional materials (implying both, tension *and compression*) was experimentally determined—although, the statement was supported by the works of Wu [22], who based the findings on tensile and shear specimens, not purely compressive loads. Another study by Konish [24] confirmed that in unidirectional tensile specimens (matrix tension), the concepts of LEFM that apply to metals can apply to fiber composites. Dharan [1] also reported the applicability of LEFM to composites under certain assumptions. Phillips [11] reached similar conclusions, showing that LEFM can be applied to laminates loaded in matrix tension. The mechanical response for the matrix in tensile loadings is well established as following the laws of LEFM, but the mechanical response of the matrix in compression is not as thoroughly explored.

2.3 Matrix Compression

A matrix compression test is similar to matrix tension, where the fibers are oriented in one direction (90°), and a (compressive) load is applied perpendicular to the fiber direction. Little work has been done to investigate matrix compression—the work of Puck et al [25] performed an analysis on fiber reinforced plastics, applying theory to reported experimental work. The investigation did not include laminates with strictly uni-directional fiber orientations, but did assume fracture surface angles of slightly higher than 45° for areas of matrix compression. This 45° fracture angle assumes that the matrix compression failure is dominated by matrix shear. It is not uncommon to assume that matrix compression damage is dominated by shear failure; with this assumption, matrix compression strain energy release rates can be (and often is) approximated as the mode II fracture toughness of the matrix [8]. Work performed by Christiansen et al [26] experimentally investigated fracture planes for CFRP composites, and observed fracture to occur along planes oriented between 31° and 38° from the loading axis (59° and 52°, respectively, measured from the through-thickness normal), which supports the shear-dominated failure assumption. Daniels [27] revealed in a literature review that there is no established method of directly measuring the strain energy release rate for matrix compression, and it is often assumed to be negligible or approximated from mode II fracture (in-plane shear). This approximation of strain energy release rate from mode II shear assumes the applicability of LEFM, but LEFM has not been proven for matrix compression. The work of Daniels [27] was meant to isolate matrix compression damage initiation and

propagation and characterize the material behaviour. Through finite element modelling, a compact compression specimen was selected for its geometric simplicity. Daniels experimentally validated the specimen with a material system having a relatively low strength ratio, $\left(\frac{\sigma_{compressive}}{\sigma_{Tensile}}\right)$ [27]. The work was continued by Rawlings et al [28], who attempted to apply Daniels's model to a different material system with a considerably larger strength ratio. Figure 1, below, shows the CC specimen reported by Rawlings that was manufactured following the work Daniels [27, 28].

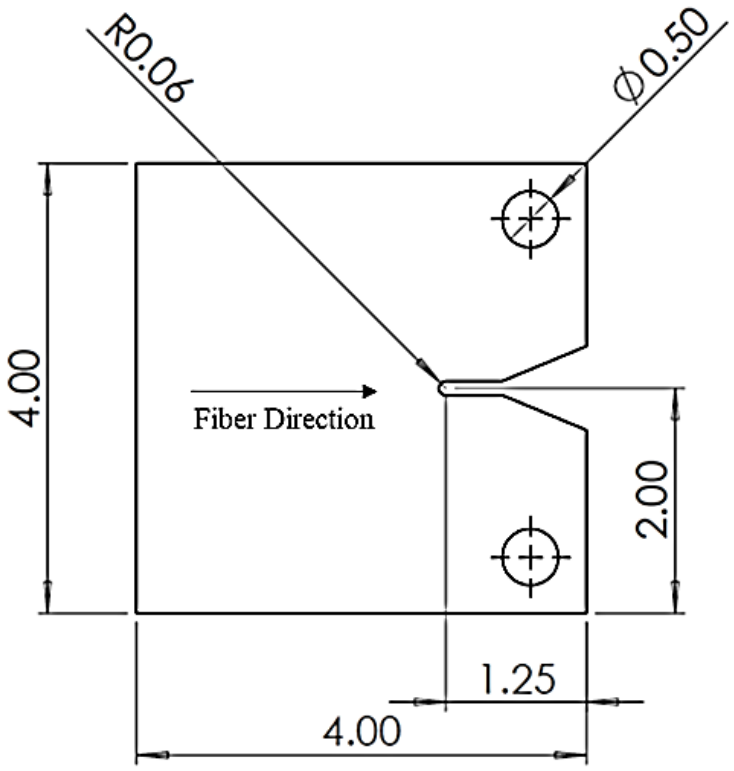

Figure 1. Compact Compression (CC) specimen of notch length 1.25-inch. Dimensions are in inches. The layup was 25-plies with fibers parallel to the notch [28].

Rawlings encountered premature matrix tension damage along the side opposing the notch tip prior to any compressive failure with the compact compression specimen suggested by Daniels. The work continued through an iterative process of compact compression specimens with fixtures, uniform compression specimens, and four- and three-point bending specimens. It was finally determined that an experimental tapered-width, uniform compression specimen, shown in Figure 2, correctly isolated matrix compression damage in the material with a large strength ratio.

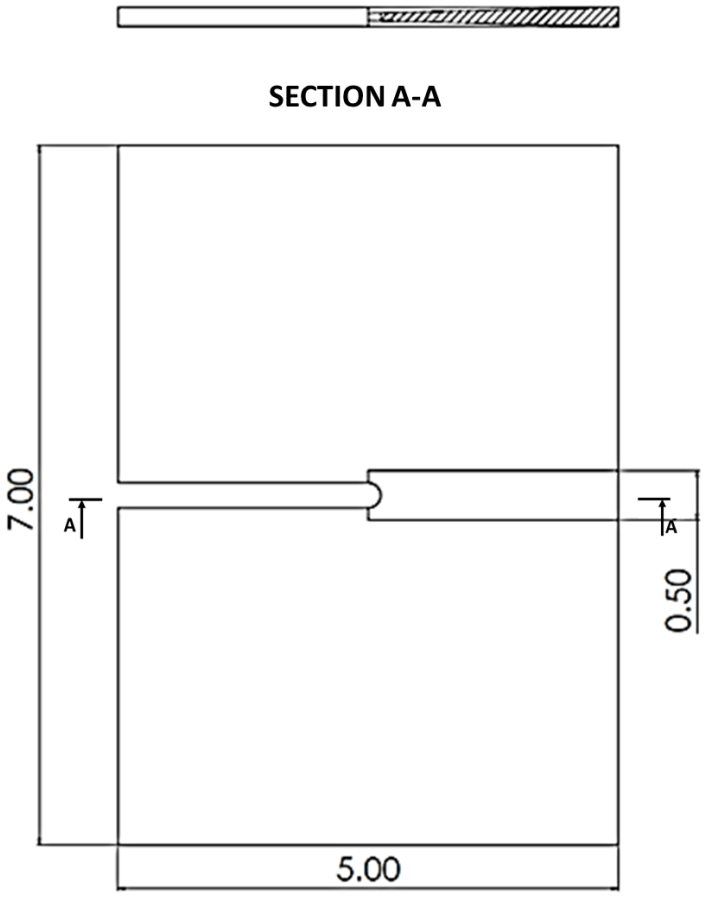

Figure 2. Rawlings's experimental tapered-width, uniform compression specimen. Dimensions are in inches. Cross-sectional view shown (top). The layup was 25-plies with fibers parallel to the notch [28].

The specimen proposed by Rawlings consisted of a machined taper though the thickness of a constant-thickness laminate; the machined taper can be unreliable for repeated manufacturing and may induce other damage. Rawlings et al [28] concluded with the suggestion that by tapering the CC specimen proposed by Daniels, a suitable specimen for matrix compression damage could be achieved for both material systems [28].

2.4 Gap in Literature

It has been shown that little work has been dedicated to matrix compression damage, and many researchers assume that the matrix is dominated by shear failure (fracture angles occurring at around ±45°). Following this assumption, the value of matrix compression strain energy release rate is approximated from the Mode II (shear) fracture toughness, which assumes that LEFM can be applied. While matrix compression fracture has been reported to occur at angles of 31°-38° from the loading axis, no studies exist to this researcher's knowledge that explore the linear elastic fracture behavior of matrix compression damage.

To investigate matrix compressive damage behavior, researchers have developed a reliable test specimen for material systems with low strength ratios [27], and an experimental specimen for material systems with large strength ratios [28]. In order to investigate the applicability of LEFM to the matrix in compression, a reliable test specimen for a range of strength ratios must be developed. It has been suggested that a non-uniform thickness Compact Compression (CC) specimen should be able to

isolate and propagate compressive damage in the CFRP composite matrix for different material systems [28].

The purpose of this research was to develop a specimen capable of the isolation and propagation of matrix compression damage in CFRP material systems with very different strength ratios, $\left(\frac{\sigma_{compressive}}{\sigma_{Tensile}}\right)$, and to investigate the applicability of LEFM to the matrix in compression. The outcomes of the study were to i) provide a test specimen capable of isolating and propagating a stable compressive crack in the CFRP matrix for a range of strength ratios; ii) prove the applicability of the laws of LEFM to the matrix in compression; and iii) to propose a method to obtain the matrix compression critical strain energy release rate.

Chapter 3

3 Experimental Specimen Selection

3.1 Introduction

Due to the complexity of composite material systems, an experimental investigation was necessary to identify a suitable test specimen. A successful specimen would isolate matrix compression damage initiation and propagation in two material systems with different strength ratios. Following the suggestions from literature, CC specimens were selected to investigate the effects of having a non-uniform thickness.

One of the largest concerns of this researcher was the possibility of machining-induced damages to the matrix. Because previous researchers machined a taper into uniform thickness specimens, it was unsettling to conclude that the specimen *geometry* caused the desired failure, and not the possibility of induced damage from the machining process. Therefore, this research sought to manufacture a variable thickness through creative layup schedules.

3.2 General Methods

The low-strength ratio material used was a Mitsubishi Rayon TR50S/NB301 carbon fiber-epoxy resin unidirectional pre-preg laminate (having a strength ratio of about 2), and the high-strength ratio material used was proprietary (with a strength ratio much greater than 2). After a laminate was cured, it was outsourced to a local company,

Viper Northwest, Inc., to have the geometry precision water-jet cut. Once the final specimen geometry was prepared, each specimen was painted a flat black, and speckled with white paint for *in-situ* image capture for tracking compressive crack growth.

All compression tests were conducted using an Instron 2580-202 30kN (6750 lb) Load Cell with an error of 0.5% on an Instron 5567 30kN (6750 lb) load frame. Compression tests were displacement-controlled at a rate of 0.04 in/min. The Instron software outputs a force-displacement plot for every test, which aided in determining if matrix compression damage was occurring—identified by a sudden load drop (damage initiation), and a relatively constant load carried over an extended displacement (the propagation of the crack). The force was measured from the load cell, and the displacement was the crosshead displacement. At the beginning of every test, the specimen was loaded into the fixture—taking care to align the specimen collinear with the load-line to prevent a moment arm, shear loading, and buckling. A pre-load of about 20 lbs was loaded through the specimen, and the displacement was set to zero. In addition to visually observing the specimen during the tests, two Point Grey Flir Grasshopper GRAS-50S5M-C cameras were used with a LavVIEW Vi to record the specimen at a rate of 7.5 fps and collect the images for later crack extension measurements.

3.3 Specimen Selection

Several iterations of CC specimens were attempted before a suitable specimen was obtained—this investigation was performed and published in collaboration with another researcher, McKinley et al [29]. The identification of a successful specimen consisted of two features: compressive damage initiation, and compressive damage propagation, both of which must have occurred prior to any other failure mode (i.e. matrix tension damage on the opposing side).

3.3.1 Machined Taper in CC Specimen with High-Strength Material

Following the suggestions of Rawlings [28], a taper was machined, using a ½" carbide end mill bit, into a pre-existing, 4-inch by 4-inch uniform thickness CC specimen of the high-strength ratio material system, to validate the isolation of matrix compression damage using the CC specimen geometry (seen in Figure 3).

Figure 3. Compact Compression specimen with a machined taper. 0.5-inch width taper, starting at the notch tip; specimen thickness increases to the left in the image. Dimensions are of those in Figure 1 [29].

The specimen exhibited the desired results (as shown in Figure 4), but the question remained: was the success a result of the taper, or machining-induced damages around the notch tip?

Figure 4. Load-displacement plot of the machined-taper specimen. Note: units and values have been removed due to proprietary nature [29].

The load-displacement plot in Figure 4 reveals that the load drops slightly on the linear portion of the curve; this is indicative of compressive crack formation, as reported in the article [29] (note that while the units and values have been omitted from the figure, the material behaviour is what is important to this part of the study). While the specimen appears to exhibit the desired failure mechanism, it was unclear if the specimen geometry or machining-induced damages caused the onset of damage. A test specimen was needed without the possibility of machining-induced damages.

3.3.2 Tapered CC Layup with Low-Strength Material

By collaborating with another researcher, another 4-inch by 4-inch CC specimen was designed to have a taper as a result of the layup process—the layup schedule and ply geometry were organized to introduce a gradual taper to the specimen with a 10-ply thin region around the notch tip, and 30-ply thick region on the opposite (tensile) side of the specimen. The specimen was modelled in Abaqus and showed promising results: compressive damage was predicted to occur prior to tensile splitting.

Because the taper was a result of the layup schedule, and individual plies were very thin, a high-precision layup mould was designed and ordered to create the desired geometry. It is worth noting that the alignment of the top plies was difficult to achieve due to the obstruction of vision caused by the other plies. The tapered specimen was manufactured using the low-strength ratio material as an affordable proof of concept, as shown in Figure 5, and tested with the Instron.

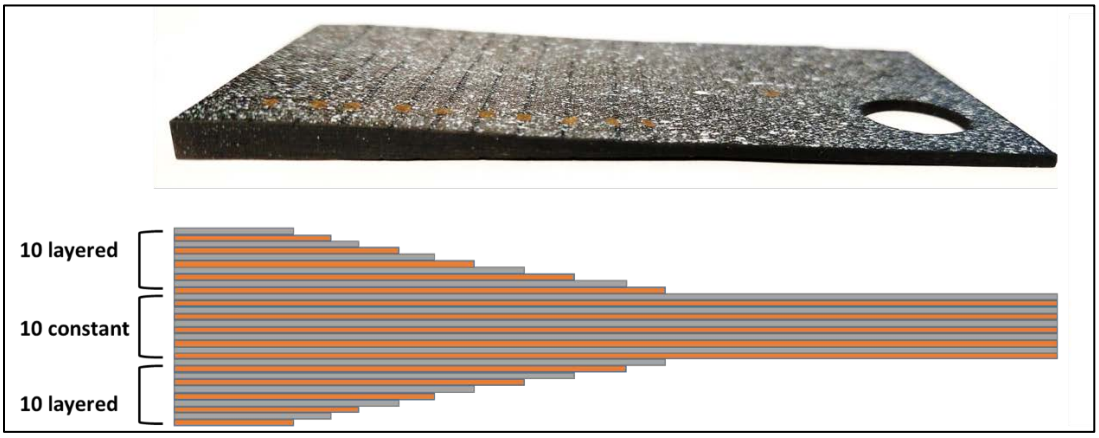

Figure 5. Tapered CC layup specimen. Notch was cut from the 10-ply thin region (right side of the image).

The geometry of the specimen consisted of a 10-ply thin region *where the load was being applied*, causing the specimen to buckle at this thin (compressive) side, and crack at the load application site. Any attempts to modify the mould to investigate potential solutions would require expensive, high-precision machining. This specimen was rejected due to its manufacturing difficulties, and undesirable failure mechanism.

3.3.3 00°-Plies CC Specimen with Low-Strength Material

To explore a simpler geometry without a complex layup schedule, the 4-inch by 4-inch uniform-thickness CC specimens were investigated once more. Recalling from literature, the high-strength ratio material would fail in premature matrix tension on the side opposite the notch; strengthening the “tensile” side could prevent the specimen from failing in tension. Ten 1-inch-wide plies were added above and below a uniform-thickness CC specimen along the tensile edge, with fibers running parallel to the loading direction (0°), as shown in Figures 6 and 7.

Figure 6. 0°-Plies CC Specimen, as viewed from the side.

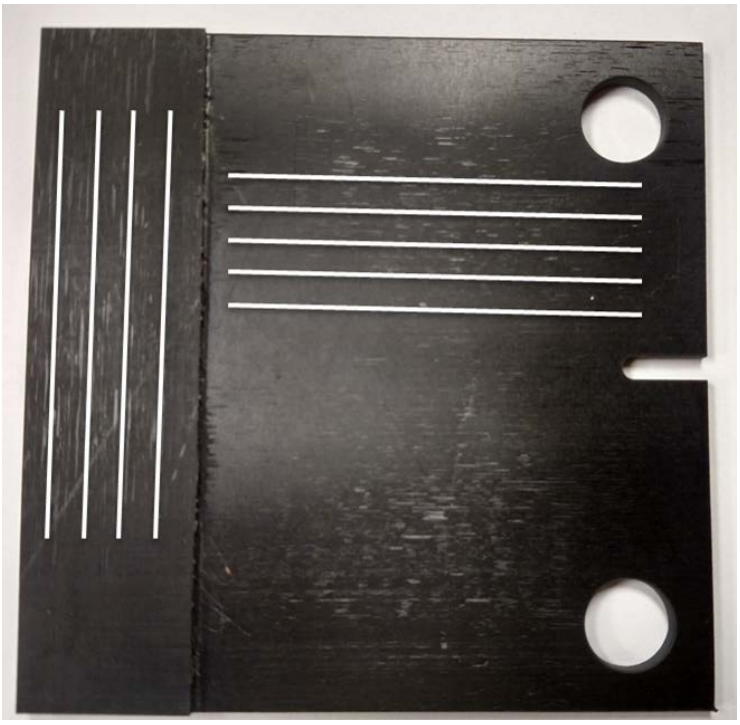

Figure 7. 0°-Plies CC Specimen, as viewed from the front. White lines indicate fiber direction in different regions of the material.

Testing with low-strength ratio material showed matrix tensile failure at the load application site, and the specimen was rejected.

3.3.4 Machined Step in CC Specimen with High-Strength Material

Because the layup taper from section 2.3.2 required precision tooling and was difficult to layup, investigation into a step—a thin (0.08-inch), constant thickness region around the notch tip—was conducted. The idea was to investigate whether the specimen needed a *taper*, or just a thinner section. The step was machined into a pre-existing, uniform thickness (0.18-inch) specimen of the high-strength ratio material using a 1-inch carbide end mill bit, shown in Figure 8, below.

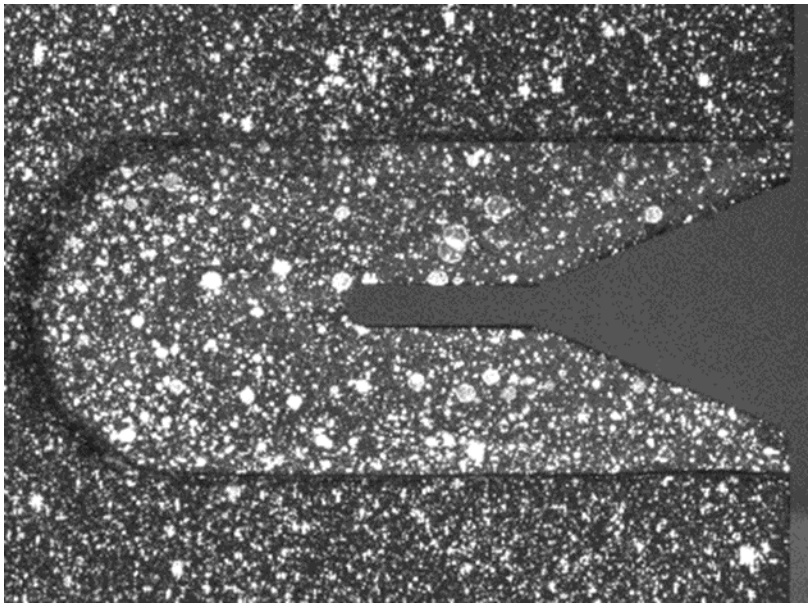

Figure 8. Machined 1-inch step specimen. Step was made in a pre-existing CC specimen of high-strength ratio material.

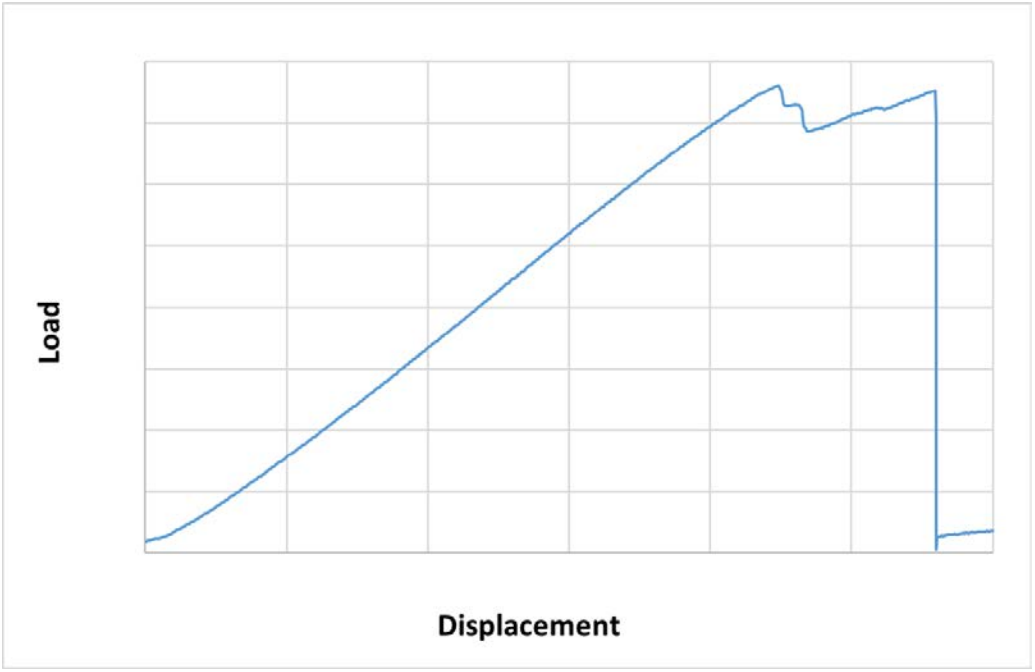

Figure 9. Load-Displacement curve of the 1-inch machined step specimen. Note: units and values have been removed due to proprietary nature.

While the compression test resulted in successful isolation of compressive damage initiation and propagation, evident by the sudden load drop along the linear portion of the curve in Figure 9, and the continued load-carrying ability, the possibility of machining-induced damages was still of concern (note, again, that while the units and values have been omitted from the figure, the behaviour is what is important for this part of the study).

3.3.5 Stepped CC Specimen with Low- and High-Strength Materials

After experimental validation that a thin, uniform-thickness region was successful, individual ply geometry, and layup tools were designed to create a manufactured 4-inch by 4-inch CC specimen with a 1-inch by 3-inch thin region at the mid-plane of the specimen, as shown in Figures 10 -11.

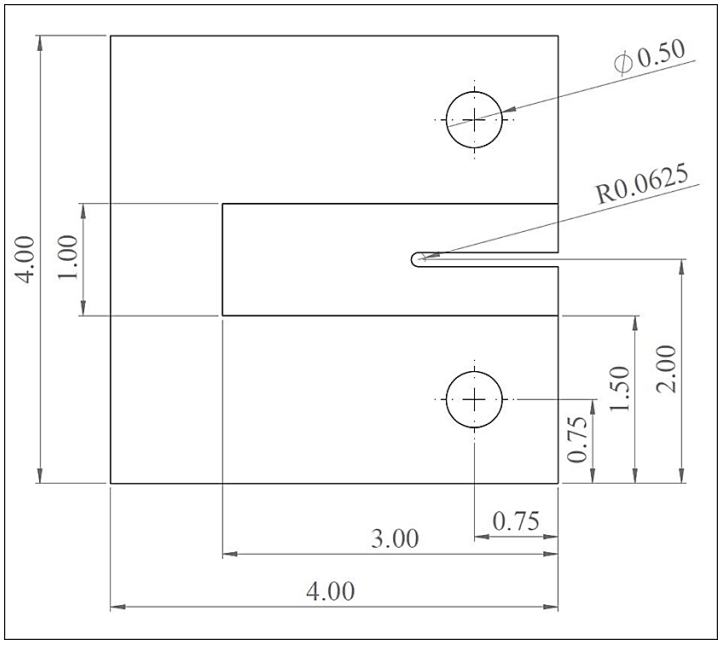

Figure 10. Final CAD drawing of Stepped specimen geometry. Dimensions are in inches. An example notch length of 1.25-inch is shown.

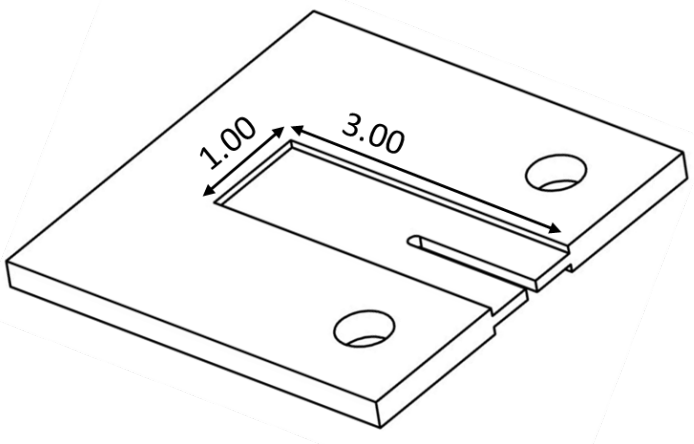

Figure 11. 3D view of Stepped specimen geometry. Dimensions are in inches.

To save costs, experimental validation of this manufactured geometry was conducted with the low-strength ratio material. The specimen was refined through testing, and

was determined that 15-plies were needed at the thin region to prevent buckling, and 35-plies at all other locations. The specimen showed successful isolation and propagation of compressive damage in the matrix for the low-strength ratio material—another researcher applied this geometry to the high-strength material and showed success with variable notch lengths.

3.4 Conclusion

The Stepped CC specimen was successful in the isolation of matrix compression damage initiation and propagation prior to any of the other three modes of failure (matrix tension, fiber compression and fiber tension) in both material systems. After experimental validation of the specimen geometry for both material systems, the remainder of this study focuses only on the mechanical behaviour of the low-strength ratio material. With a suitable test specimen to isolate the desired damage, an investigation to the material response could be conducted, and is discussed in Chapter 4.

Chapter 4

4 Applicability of Linear Elastic Fracture Mechanics

4.1 Background

Fracture mechanics involves the investigation of the failure of materials, and how to predict premature failure [30]. In a traditional (simple) approach to the strength of materials, one can relate a material's ability to withstand an applied stress to its properties (yield strength, or tensile strength); Fracture mechanics relates the applied stress to the material's fracture toughness, and a flaw size. *Linear Elastic* Fracture Mechanics (LEFM) is applicable to materials that obey Hooke's law, and was the foundation of the development of fracture mechanics. Under the restrictions of linear elasticity, an equation for the failure stress (or load) that a part with a crack could support was developed and is called the Griffith equation. One form of the Griffith equation is shown in Equation 1:

$$\sigma_f = \left(\frac{2E\gamma_s}{\pi a}\right)^{1/2} \quad (1)$$

Where σ_f is the applied stress at failure (the maximum stress the material can withstand until it fails), E is Young's modulus, γ_s is the surface energy of the material, and a is the crack half-length. Of course, Equation 1 is often generalized for *any* type of fracture behaviour (plastic, visco-elastic, etc.) by replacing γ_s with w_s, where w_s is the material's fracture energy. What is important to note is the dependence of the

failure load to the crack half-length raised to the (-0.5) power. Recognizing that the applied stress, σ_f, is equal to the applied force divided by the area over which the force is applied, and by collecting the constant terms in Equation 1, and identifying them as *C*, Equation 2 can be obtained through mathematical manipulation of Equation 1:

$$\log(F_f) = C - 0.5\log(a) \quad (2)$$

Where F_f is the failure load. It is evident that a log-log plot of the failure load vs the crack half-length should yield a linear relationship with a slope of -0.5, if a material follows LEFM.

4.2 Methods

To investigate the applicability of LEFM to the commercial (low-strength ratio) material, specimens of the geometry described in Section 3.3.5, and shown in Figure 10 were mass manufactured with varying initial notch lengths. Fourteen (14) different initial notch lengths were explored, with three (3) specimens manufactured for each notch length. Following the testing procedures in Section 3.2, load-displacement curves were generated for each specimen, and image data was collected for tracking the compressive crack progression. An image of a Stepped specimen is shown in Figure 11, below.

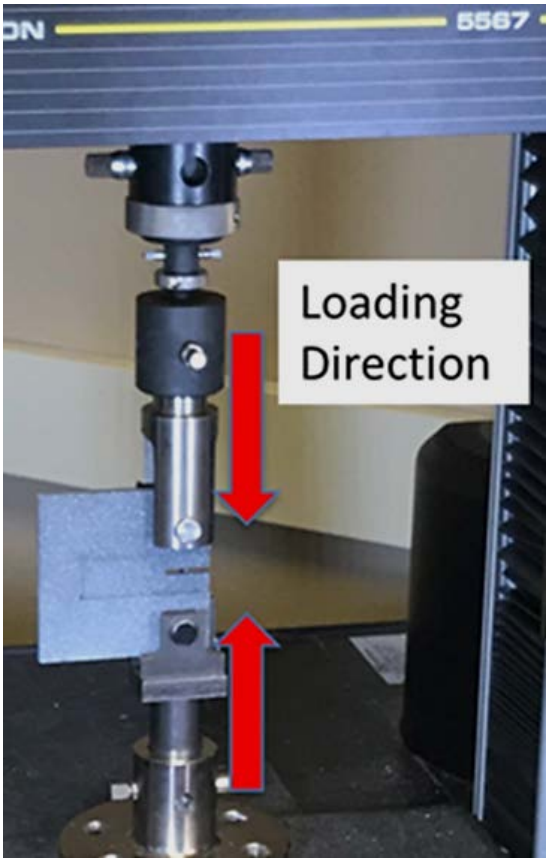

Figure 12. Stepped Specimen loaded in the Instron. The loading direction is indicated by red arrows.

For notch lengths ranging from 0.25-inch (Figure 12a) to 1.875-inch (Figure 12b) at 0.125-inch increments, it was determined that at the longest notch length investigated (1.875-inch), the geometry of the material no longer exhibited compressive damage prior to tensile splitting along the opposing edge, thus, data was reported only for notch lengths between 0.25-inch and 1.75-inch. Similarly, data at notch lengths of 1.125-inch and 1.5-inch were not reported due to poor specimen behaviour during the tests—sensitivity of the specimens to alignment in the test fixture, as well as any manufacturing defects present in the material (delamination, voids, particles, etc.) led

to unwanted failure mechanisms (premature tensile damage prior to compressive damage, mode III: out-of-plane shear, or buckling) in the specimens. After omitting the data from the 1.875-inch, 1.125-inch, and 1.5-inch notch lengths, the data pool consisted of eleven (11) different notch lengths, with three (3) specimens at each notch length, resulting in a total of 33 data points for analysis.

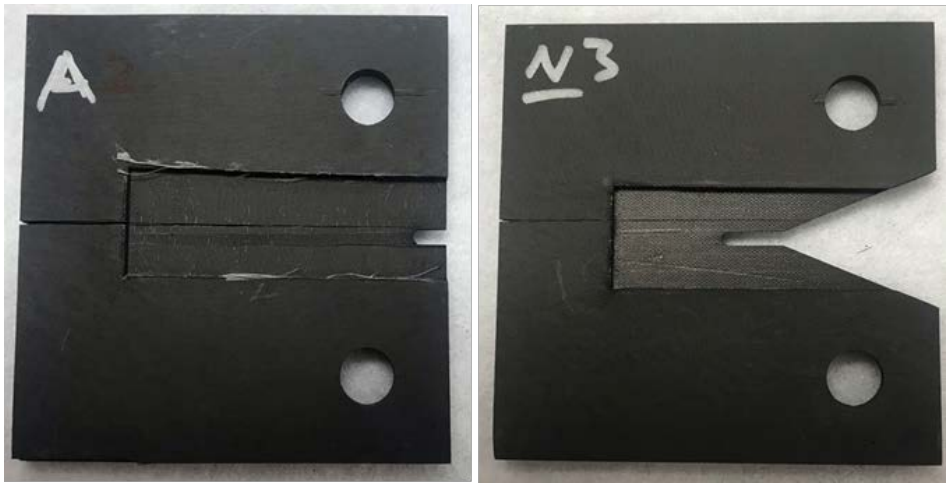

Figure 13. (a) Stepped CC specimen with 0.25-inch notch (left); (b) Stepped CC specimen with 1.875-inch notch (right). Images taken after testing, viewed from the back-side (non-speckled).

In Equation 2, *a* represents the crack *half-length*, but for edge notches (such as those in the specimen geometry used here), *a* is the length of the notch. The analysis of the load-displacement output data from the Instron software identified the failure load for each test specimen—the maximum load applied during the test before damage initiated (identified by a sudden drop in the applied load due to a decrease in material stiffness after damage). The peak loads for each test were collected, and the logarithm of each load was plotted against the logarithm of its corresponding initial notch length

in Microsoft Excel. This plot, for LEFM, would follow a linear trend, showing the relationship between failure load and notch length as governed by the logarithmic manipulation of the Griffith equation (Equation 1), shown in Equation 2. Upon closer inspection of Equation 2, one can see that it has the form of the slope-intercept equation, $y=mx+b$, where *'y'* would be $log(F_f)$, and *'x'* would be $log(a)$, the slope, m, would be -0.5, and the y-intercept, *'b,'* would be the constant terms, C.

4.3 Results

Typical load-displacement curves for select notch lengths are shown in Figures 13-15, and described below.

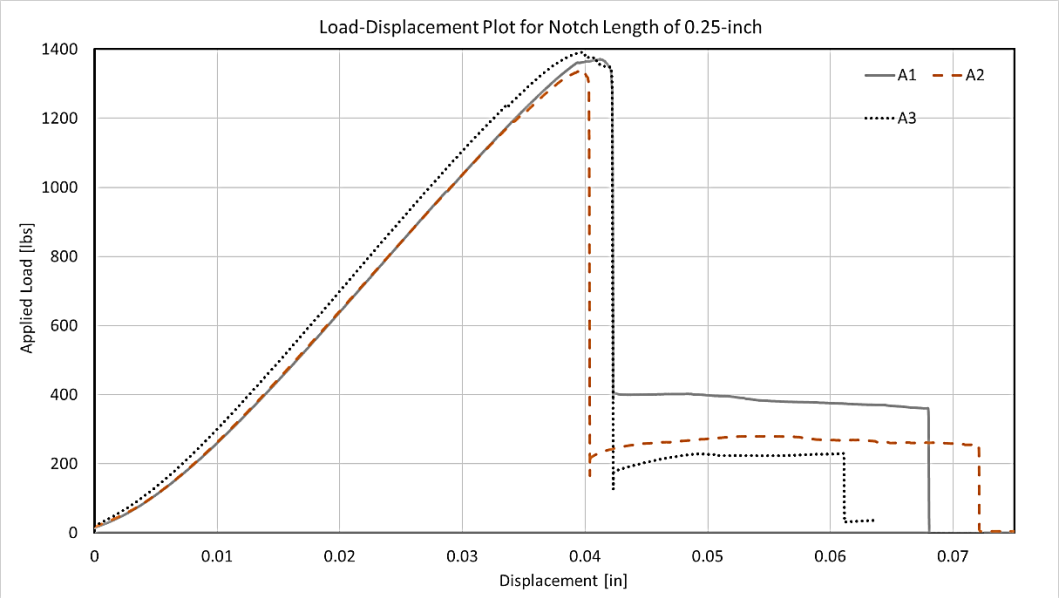

Figure 14. Load-Displacement plot for the three specimens having a notch length of 0.25-inch. Specimens identified as A1, A2, and A3.

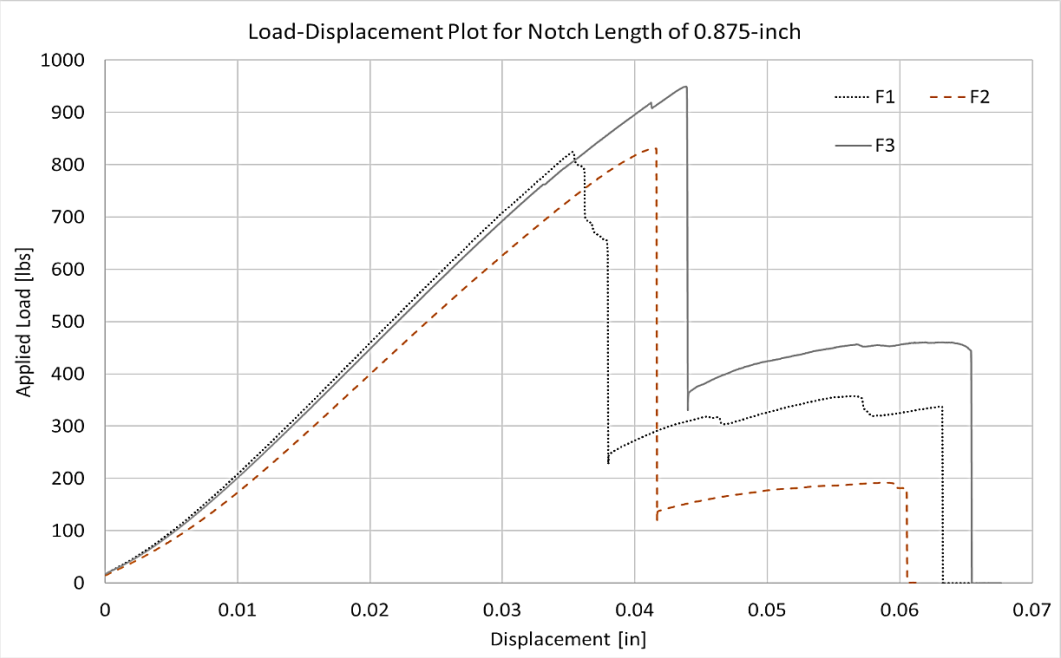

Figure 15. Load-Displacement plot for the three specimens having a notch length of 0.875-inch. Specimens identified as F1, F2, and F3.

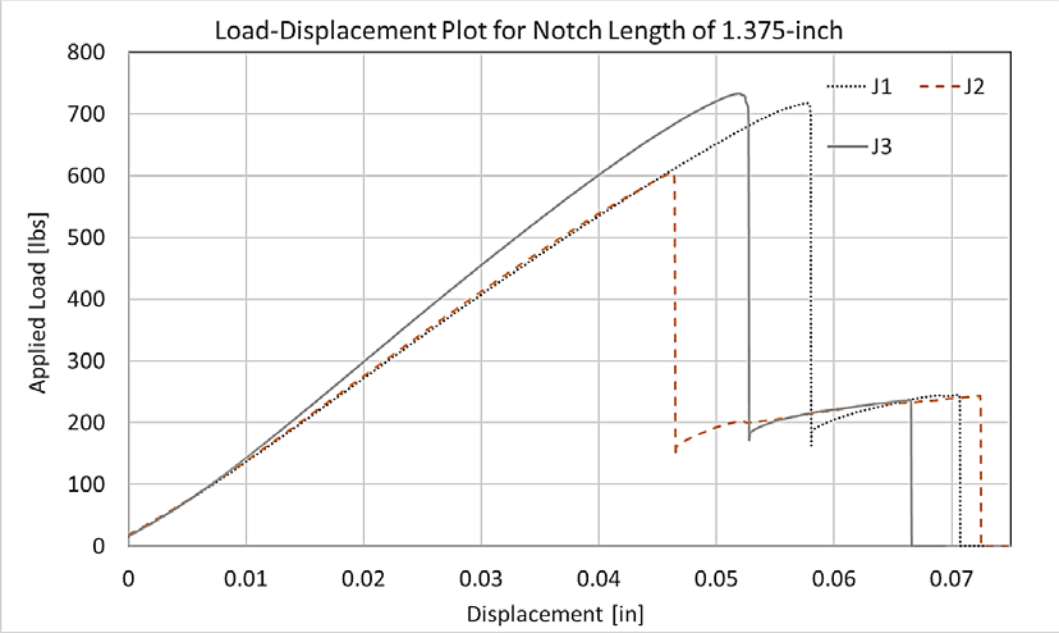

Figure 16. Load-Displacement plot for the three specimens having a notch length of 1.375-inch. Specimens identified as J1, J2, and J3.

Figures 13-15 show typical load-displacement curves that were generated during the variable notch length investigation. It can be seen that all of the plots have the same key features, which are identified in Figure 16, below: a linear increase in load (region A), a maximum applied load (point B) just before the compressive damage initiated, a sudden drop in load (between points B and C) due to a decrease in material stiffness caused by damage *initiation*, continued load-carrying ability after the load drop (region D) during compressive damage *propagation*, and a final drop in load to zero (point E) when the specimen had cracked into two pieces from tensile splitting.

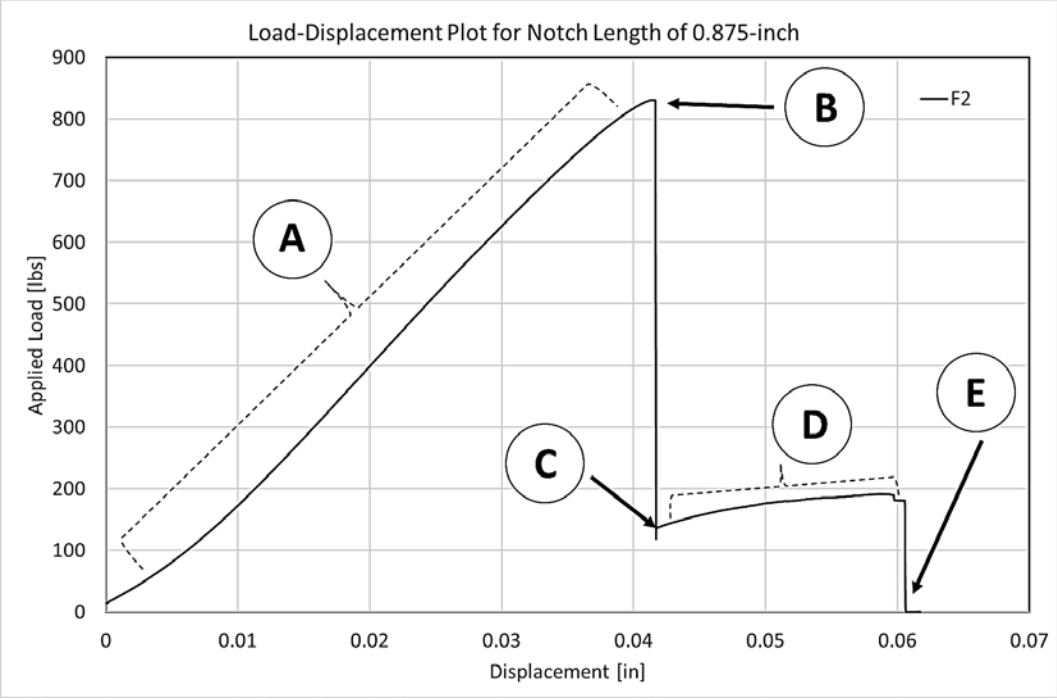

Figure 17. Load-Displacement plot for behaviour identification. The plot reflects test specimen F2, with 0.875-inch notch length.

The maximum applied load that initiated compressive damage, or "failure load," for each specimen with the corresponding notch lengths are shown in Table 1, below.

From the table, it can be seen that as the notch lengths increase, the corresponding failure loads appear to decrease, as expected for linear elastic materials.

Table 1. Failure load data (in pounds) from the Instron for each of the specimens, with corresponding initial notch lengths (in inches).

Specimen Identifier	Initial Notch Length [in]	Failure Load [lbs]
A1	0.25	1370.99
A2	0.25	1340.54
A3	0.25	1391.31
B1	0.375	1278.29
B2	0.375	1388.31
B3	0.375	1217.99
C1	0.5	1331.76
C2	0.5	1227.04
C3	0.5	1052.09
D1	0.625	1178.62
D2	0.625	1026.52
D3	0.625	1085.76
E1	0.75	957.74
E2	0.75	1119.93
E3	0.75	1092.63
F1	0.875	824.67
F2	0.875	830.53
F3	0.875	949.81
G1	1.0	829.48
G2	1.0	599.18
G3	1.0	1098.36
I1	1.25	771.39
I1	1.25	628.43
I3	1.25	803.91
J1	1.375	717.82
J2	1.375	604.12
J3	1.375	733.62
L1	1.625	523.68
L2	1.625	540.08
L3	1.625	567.54
M1	1.75	501.72
M2	1.75	451.48
M3	1.75	470.05

From the data in Table 1, the log-log plot discussed above was generated, and is shown in Figure 17, below. From this plot, a linear trend is observed with an R^2 value of about 0.83 (meaning that the linear trend line models 83% of the variability in the data), and a slope of about -0.54. A residual plot further confirmed the appropriateness of a linear fit to the data.

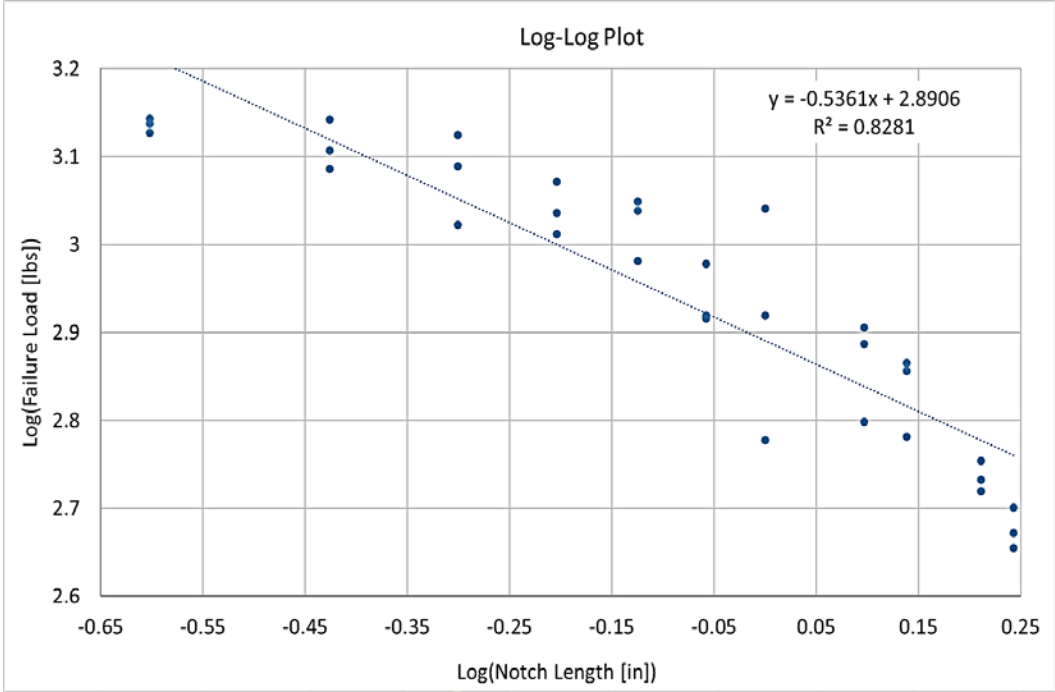

Figure 18. Log-log plot of failure load versus corresponding notch length. Linear regression line is shown as dotted line, with equation in upper right corner.

Error bars were added to the plot shown in Figure 17, with values equal to the absolute value of the maximum of the differences between the linear trend line and the data points at each notch length (Equation 3, below).

$$Error = \pm \max \left| y_{fitted,i} - y_{data,i} \right| \quad (3)$$

Where *i* is the data point at each notch length (*i* = 1, 2, 3), y_{fitted} is the value of $\log(F_f)$ on the trend line, and y_{data} is the value of $\log(F_f)$ from the experimental data. The theoretical line (from Equation 2) having a slope of -0.5, and using the same y-intercept as the fitted line was plotted onto the pre-existing figure, and is seen in Figure 18, below.

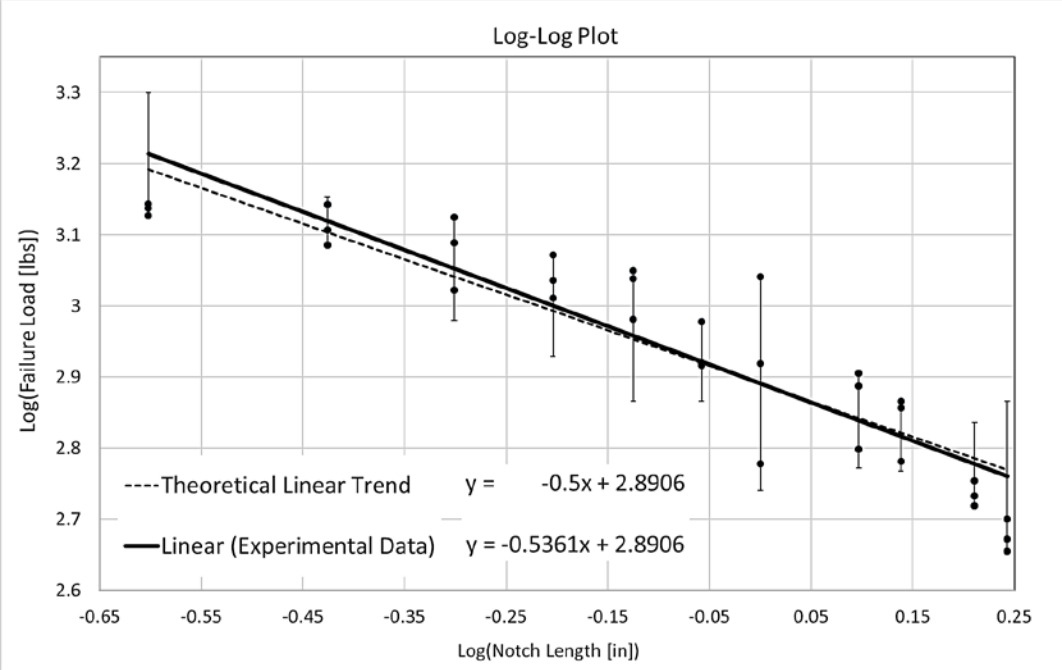

Figure 19. Log-log plot with theoretical line overlaid on fitted curve and error bars. Theoretical line is dotted, fitted line is solid.

From Figure 18, it can be seen that the LEFM relationship described in Equation 2 which reflects a linear trend of the logarithm of failure load against the logarithm of notch length with a slope of -0.5 fits within the error bars of the fitted trend line to the experimental data. The linear trend observed in Figure 17 (with a slope of approximately -0.54) indicates that the matrix, under compressive loading, follows

the relationship described by Equation 2, which concludes that LEFM can be applied to this material.

Chapter 5

5 Obtaining the Matrix Compression Strain Energy Release Rate

5.1 Background

In addition to the dependence of failure load on flaw size and fracture toughness of a material, Linear Elastic Fracture Mechanics introduces the concept of energy release rate—the energy required for a crack to initiate/propagate a unit distance [30]. This value is used as an input parameter in current damage models (e.g. continuum damage mechanics models), and many industries will assume this value to be negligible, equivalent to the matrix tension value, or approximated from mode II (shear).

Similar to the model used to develop the Griffith approach to fracture, the energy release rate, denoted as $\mathcal{G}$, was developed and is defined as the energy per unit crack extension; it is the change in potential energy with respect to crack area, and can be written in terms of forces and displacements:

$$\mathcal{G}_c = -\frac{\Delta}{2B}\left(\frac{dF}{da}\right)_{\Delta} \tag{3}$$

Where *dF* is the drop in applied load, *a* is the crack extension, and Δ is the displacement. *B* is the width of the specimen, but, in reality, it is the crack surface width, and when multiplied by 2 and *da*, the total crack surface area formed from the

fracture is obtained. The subscript *c* on the strain energy release rate term in the above equation refers to the critical value when a crack would extend. It is worth noting that that Equation 3 is for displacement-controlled loading (as was performed in this research), but can also be written to accommodate fixed loading situations. Using Equation 3 and the load-displacement plots generated during the tests, the strain energy release rate for the material was calculated. This value of critical strain energy release rate is considered a material property, and should be reflected in the calculations presented below by a steady value, regardless of initial notch length or failure load.

5.2 Methods

Before the tests, the specimens were spray-painted a flat black color and speckled with white paint. During the tests, images were collected of the surface of the speckled specimens, in order to track the rapidly advancing crack that formed at the failure load. In Equation 3, F and Δ are outputs from the Instron (dF is obtained by subtracting the failure load from the load immediately following fracture), and da and B are the only remaining unknowns. These unknown values were obtained by measuring the specimen with calipers.

At the failure load, a crack would suddenly form and extend a distance, da, and the speckle pattern was used to identify where the crack tip was. To measure da, the images collected on each specimen were analyzed to determine how far the crack extended. The location of the crack tip with respect to the speckle pattern from the

images was determined on the specimen, and calipers were used to measure the distance of the formed crack.

Similarly, the crack surface width, *B*, was measured with calipers across the thickness of the specimen, following the path of the crack surface through the thickness. Using Equation 3, the critical strain energy release rate was calculated.

5.3 Results

From the data calculated and displayed in Table 2, an average critical strain energy release rate, $\mathcal{G}_c$, was calculated to be 65.51-lb/in with a standard deviation of about 18.66-lb/in. This value compares with Daniels [27], who was reporting a value of 35-lb/in for the same material system (calculated using a different equation, called the Compliance Calibration Equation). Considering the spread in the data and the crude methods used to obtain the crack extension, *da*, and crack surface width, *B*, it must be acknowledged that the average $\mathcal{G}_c$ obtained here is a very rough value, and other methods exist for a more reliable determination, such as the J-integral calculation from Digital Image Correlation (DIC) or strain gauges on the specimen.

Table 2. Values from the load-displacement data generated with the Instron, as well as the crack surface widths and crack extensions, and calculated strain energy release rates.

Specimen Identifier	Initial Notch Length [in]	Failure Load [lbs]	Load after Failure [lbs]	*dF* [lbs]	Δ [in]	*da* [in]	*B* [in]	$\mathcal{G}$ [lbs/in]
A1	0.25	1370.99	387.23	983.76	0.041	2.27	0.086	104.69
A2	0.25	1340.54	165.29	1175.25	0.040	2.29	0.175	58.50
A3	0.25	1391.31	125.44	1265.87	0.040	2.38	0.148	71.44
B1	0.375	1278.29	384.74	893.56	0.040	2.11	0.105	79.56
B2	0.375	1388.31	296.78	1091.53	0.041	2.26	0.131	76.75
B3	0.375	1217.99	104.52	1113.48	0.038	1.88	0.115	97.25
C1	0.5	1331.76	117.59	1214.16	0.042	2.36	0.157	68.93
C2	0.5	1227.04	113.32	1113.72	0.039	2.06	0.138	76.40
C3	0.5	1052.09	75.44	976.65	0.041	2.13	0.172	55.42
D1	0.625	1178.62	889.70	288.91	0.041	0.84	0.220	32.44
D2	0.625	1026.52	506.99	519.52	0.036	0.88	0.139	77.23
D3	0.625	1085.76	123.03	962.73	0.039	2.63	0.150	47.33
E1	0.75	957.74	284.74	672.99	0.040	1.69	0.103	77.53
E2	0.75	1119.93	117.96	1001.98	0.043	1.94	0.148	75.19
E3	0.75	1092.63	73.37	1019.26	0.043	2.13	0.139	73.32
F1	0.875	824.67	227.87	596.80	0.035	1.46	0.128	56.71
F2	0.875	830.53	118.69	711.84	0.041	1.91	0.106	73.01
F3	0.875	949.81	330.78	619.02	0.044	1.75	0.143	54.22
G1	1.0	829.48	269.95	559.53	0.044	0.88	0.125	112.31
G2	1.0	599.18	295.76	303.42	0.033	0.75	0.130	51.26
G3	1.0	1098.36	98.18	1000.18	0.051	1.85	0.190	73.17
I1	1.25	771.39	105.83	665.57	0.048	1.63	0.138	71.83
I1	1.25	628.43	140.97	487.45	0.039	1.50	0.161	39.14
I3	1.25	803.91	122.60	681.31	0.050	1.68	0.218	46.71
J1	1.375	717.82	162.58	555.24	0.058	1.44	0.165	67.64
J2	1.375	604.12	145.33	458.79	0.046	1.44	0.128	57.76
J3	1.375	733.62	172.15	561.46	0.052	1.38	0.143	74.58
L1	1.625	523.68	118.74	404.93	0.045	1.25	0.136	53.79
L2	1.625	540.08	285.95	254.13	0.049	1.88	0.109	30.67
L3	1.625	567.54	122.80	444.74	0.052	1.25	0.173	53.38
M1	1.75	501.72	114.58	387.14	0.053	1.06	0.122	78.58
M2	1.75	451.48	228.67	222.81	0.046	1.00	0.136	37.91
M3	1.75	470.05	125.19	344.85	0.057	1.31	0.131	57.05

Chapter 6

6 Conclusion

This research sought to address two important gaps in literature: the lack of a test specimen to successfully isolate compressive damage in the matrix of carbon fiber reinforced plastic (CFRP) laminates with a range of strength ratios $\left(\frac{\sigma_{compressive}}{\sigma_{Tensile}}\right)$; and to validate the applicability of linear elastic fracture mechanics (LEFM) to the CFRP matrix in compression. The first part of this investigation used an experimental approach based on existing literature to identify a test specimen that was capable of isolating compressive damage initiation and propagation in the CFRP matrix. The second study used the developed test specimen to investigate the material response and compare the response with LEFM relationships.

Following the suggestions proposed in literature, specimens were explored for the isolation of matrix compression damage. A successful specimen was identified when a compressive crack formed at the tip of a notch prior to any other forms of damage, and the crack progressed stably through the specimen. A final 4-inch by 4-inch compact compression (CC) specimen was identified that consisted of a thin region (15-plies) near the notch, and 35-plies everywhere else. The thin region was 1-inch tall, and 3-inches long and was located along the notched edge of the specimen, at the mid-plane of the specimen. These specimens showed successful isolation of compressive damage in both the low-strength ratio commercial material (Mitsubishi

Rayon TR50S/NB301 carbon fiber-epoxy resin unidirectional pre-preg laminate), and the high-strength ratio proprietary material.

After the identification of a successful test specimen, an investigation into the applicability of LEFM was conducted with variable notch lengths. Using eleven (11) notch lengths, and three (3) specimens per notch length (for a total of 33 test specimens), a log-log plot of the failure load and initial notch length was generated. This plot was expected from LEFM to be linear with a negative slope of 0.5, and the data exhibited a linear trend with a slope of -0.54. The LEFM relationship was plotted over the experimental data with error bars on the fitted line, and was within the acceptable range; it was concluded that the assumption of the applicability of LEFM to the matrix of the low-strength ratio CFRP material system was valid.

In addition to addressing the gaps in literature, a method was proposed to obtain the matrix compression critical strain energy release rate. An average value of 65.51-lb/in with a standard deviation of about 18.66-lb/in was calculated from the load-displacement plots from the data pool. While the value compared with previously reported values for the same material system [27], the methods used to obtain certain parameters—the crack length and crack surface width—were crude: reference images coupled with a speckled paint pattern and caliper measurements of a crack. Other, more reliable, methods for obtaining the critical strain energy release rate exist, such as the J-integral, which uses Digital Image Correlation (DIC) or strain gauges to obtain strain fields around a crack tip, and then relates the surface displacements/strains to the strain energy in the material [30]. These measurement techniques can be combined with the test specimen reported here to obtain the value

for matrix compression. Current models (e.g. the continuum damage mechanics models) require the matrix compression critical strain energy release rate as a material property input parameter, and many industries will assume the value to be negligible, or use the matrix tension value. With CFRP's, it is intuitive to think of the plastic matrix to be much stronger in compression than in tension, rendering these assumptions invalid. With the test specimen and method proposed in this research to calculate such a parameter, models can be used more effectively for accurate interpretation of results.

On the subject of more accurate models, the continuum damage mechanics model currently treats the stiffness as a linear degradation to zero after the onset of compressive damage, which is not intuitive. After compressive damage initiates, one would think that as the two fractured surfaces are being forced into one another, the two faces would exhibit (after the sudden drop from the damage initiation) an increase in load-carrying ability, or a sustained load, not a linear trend to zero. It was consistently observed that the matrix continued to carry load after damage initiated, seen in the load-displacement curves after the onset of damage (Figures 13-16); as the crack propagated, the load remained relatively stable.

Future work on this subject would include a comparative study between energy release rate calculation methods, the development of a new material model—one that reflects the observed post-damage initiation behaviour—and implementation into modelling software. With the test specimen reported here, one could extend this variable notch length study into a mixed-mode loading investigation, and explore the concepts of stress intensity factors to further validate the applicability of LEFM.

Bibliography

[1] C.K.H. Dharan, “Fracture Mechanics of Composite Materials,” *Journal of Engineering Materials and Technology*, vol. 100, pp. 233-247, 1978.

[3] I. Lapczyk, J. Hurtado, “Progressive Damage Modeling in Fiber-Reinforced Materials,” *Composites Part A: Applied Science and Manufacturing*, vol. 38, no. 11, pp. 2333-2341, 2007.

[3] M. Langley, "Carbon Fibres- The First Five Years (Carbon Fiber Reinforced Plastics, Considering Aerospace and Medical Applications)" *Flight International*, vol. 100, pp. 406-408, 1971.

[4] S.T. Pinho, C.G. Davila, P.P. Camanho, L. Iannucci, P. Robinson, “Failure Models and Criteria for FRP Under In-Plane or Three-Dimensional Stress States Including Shear Non-Linearity,” 2005.

[5] J.L. Chaboche, “Continuous Damage Mechanics—A Tool to Describe Phenomena Before Crack Initiation,” *Nuclear Engineering and Design*, vol. 64, no. 2, pp. 233-247, 1981.

[6] S. Murakami, “Notion of Continuum Damage and its Application to Anisotropic Creep Damage Theory,” *Journal of Engineering Materials and Technology*, vol. 105, no. 2, pp. 99-105, 1983.

[7] Z. Hashin, “Failure Criteria for Unidirectional Fiber Composites,” *Journal of Applied Mechanics*, vol. 47, pp. 329-334, 1980.

[8] S.T. Pinho, P. Robinson, L. Iannucci, “Fracture Toughness of the Tensile and Compressive Fibre Failure Modes in Laminated Composites,” *Composites Science and Technology,* vol. 66, no. 13, pp. 2069-2079, 2006.

[9] C. Soutis, P.T. Curtis, N.A. Fleck, “Compressive Failure of Notched Carbon Fibre Composites,” *Proceedings: Mathematical and Physical Sciences,* vol. 440, No. 1909, pp. 241-256, 1993.

[10] M.P.F. Sutcliffe, N.A. Fleck, “Microbuckle Propagation in Carbon Fibre-Epoxy Composites,” *Acta metal. Mater.*, vol. 42, no. 7, pp. 2219-2231, 1994.

[11] D.C. Phillips, “The Fracture Mechanics of Carbon Fibre Laminates,” *Journal of Composite Materials,* vol. 8, no. 2, pp. 130-141, 1974.

[12] N.A. Fleck, P.M. Jelf, P.T. Curtis, “Compressive Failure of Laminated and Woven Composites,” *Journal of Composites Technology & Research,* vol. 17, no. 3, pp. 212-220, 1995.

[13] M.P.F Sutcliffe, N.A. Fleck, “Microbuckle Propagation in Fibre Composites,” *Acta Mater.*, Vol. 45, no. 3, pp. 921-932, 1997.

[14] S.H. Lee, A.M. Waas, “Compressive Response and Failure of Fiber Reinforced Unidirectional Composites,” *International Journal of Fracture,* vol. 100, pp. 275-306, 1999.

[15] S. Pimenta, R. Gutkin, S.T. Pinho, P. Robinson, “A Micromechanical Model for Kink-band Formation: Part I – Experimental study and Numerical Modelling,” *Composites Science and Technology,* vol. 69, pp. 948-955, 2009.

[16] S. Pimenta, R. Gutkin, S.T. Pinho, P. Robinson, “A Micromechanical Model for Kink-band Formation: Part II – Analytical Modelling,” *Composites Science and Technology*, vol. 69, pp. 956-964, 2009.

[17] R. Gutkin, S.T. Pinho, P. Robinson, P.T. Curtis, “On the Transition From Shear-Driven Fibre Compressive Failure to Fibre Kinking in Notched CFRP Laminates Under Longitudinal Compression,” *Composites Science and Technology*, vol. 70, pp. 1223-1231, 2010.

[18] M.J. Laffan, S.T. Pinho, P. Robinson, L. Iannucci, A.J. McMillan, “ Measurement of the Fracture Toughness Associated With the Longitudinal Fibre Compressive Failure Mode of Laminated Composites,” *Composites: Part A,* vol. 43, pp. 1930-1938, 2012.

[19] S.T. Pinho, R. Gutkin, S. Pimenta, N.V. De Carvalho, P. Robinson, “On Longitudinal Compressive Failure of Carbon-Fibre-Reinforced Polymer: From Unidirectional to Woven, and from Virgin to Recycled,” *Phil. Trans. R. Soc. A*, vol. 370, pp. 1871-1895, 2012.

[20] S.N. Nair, A. Dasari, C.Y. Yue, S. Narasimalu, “Failure Behavior of Unidirectional Composites Under Compression Loading: Effect of Fiber Waviness,” *Materials*, vol. 10, no. 8, p. 909, 2017.

[21] M.J. Laffan, S.T. Pinho, P. Robinson, A.J. McMillan, “Translaminar Fracture Toughness Testing of Composites: A Review,” *Polymer Testing*, vol. 31, pp. 481-489, 2012.

[22] E.M. Wu, “Application of Fracture Mechanics to Anisotropic Plates,” *Journal of Applied Mechanics*, vol 34, no. 4, pp. 967-974, 1967.

[23] M.E. Waddoups, J.R. Eisenmann, B.E. Kaminski, “Macroscopic Fracture Mechanics of Advanced Composite Materials,” *Journal of Composite Materials,* vol. 5, p. 446, 1971.

[24] H.J. Konish, “A Study of Fracture Phenomena in Fiber Composite Laminates,” Doctor of Philosophy, Mechanical Engineering, Carnegie-Mellon University, Pittsburgh, Pennsylvania, 1973.

[25] A. Puck, H. Schurmann, “Failure Analysis of FRP Laminates by Means of Physically Based Phenomenological Models,” *Failure Criteria in Fibre-Reinforced-Polymer Composites*, pp. 832-873, 2004.

[26] R. Christiansen, S. DeTeresa, “Failure Plane Orientations for Transverse Loading of a Unidirectional Fiber Composite,” International Journal of Solids and Structures, vol. 45, no. 25, pp. 7055-7062, 2003.

[27] M.A. Daniels, “Experimental Classification of Intralaminar Matrix Compression Damage Propagation in Carbon Fiber Reinforced Polymers,” Master of Science, Mechanical Engineering, Oregon State University, Corvallis, Oregon, 2016.

[28] T.J. Rawlings, K.T. Carpenter, J.P. Parmigiani, “Experimental Specimen for Classification of Matrix Compression Damage in Carbon Fiber Reinforced Polymers,” *ASME 2018 International Mechanical Engineering Congress and Exposition*. American Society of Mechanical Engineers, Pittsburg, Pennsylvania, 2018.

[29] T.A. McKinley, K.T. Carpenter, J.P. Parmigiani, "Development of Novel Compact Compression Specimen for Matrix Compression Damage Initiation and Propagation Behavior in Fiber Reinforced Composites," *ASME 2018 International Mechanical Engineering Congress and Exposition*. American Society of Mechanical Engineers, Pittsburg, Pennsylvania, 2018.

[30] T.L. Anderson, Fracture Mechanics: Fundamentals and Applications, Boca Raton, Florida: Taylor & Francis Group, 2005.